Does carbon nanotube buckypaper affect mode-I and II interlaminar fracture toughness under quasi-static loading?

de Paula Santos, Luis Felipe; Monticeli, Francisco Maciel; Ribeiro, Bruno; Costa, Michelle Leali; Alderliesten, René; Botelho, Edson Cocchieri

DOI
10.1016/j.compstruct.2023.117507

Publication date
2023

Document Version
Final published version

Published in
Composite Structures

Citation (APA)
de Paula Santos, L. F., Monticeli, F. M., Ribeiro, B., Costa, M. L., Alderliesten, R., & Botelho, E. C. (2023). Does carbon nanotube buckypaper affect mode-I and II interlaminar fracture toughness under quasi-static loading? *Composite Structures*, *323*, Article 117507. https://doi.org/10.1016/j.compstruct.2023.117507

Composite Structures 323 (2023) 117507

Contents lists available at ScienceDirect

Composite Structures

journal homepage: www.elsevier.com/locate/compstruct

Does carbon nanotube buckypaper affect mode-I and II interlaminar fracture toughness under quasi-static loading?

Luis Felipe de Paula Santos [a,b,*], Francisco Maciel Monticeli [c], Bruno Ribeiro [b,d], Michelle Leali Costa [a,b], René Alderliesten [c], Edson Cocchieri Botelho [a]

[a] São Paulo State University (UNESP), School of Engineering and Science, Department of Materials and Technology, Guaratingueta, Brazil
[b] Institute for Technological Research (IPT), Lightweight Structures Laboratory, Sao Jose dos Campos, Brazil
[c] Delft University of Technology (TU-Delft), Aerospace Engineering, Structural Integrity & Composites, Delft, Netherlands
[d] Federal University of Sao Paulo (UNIFESP), Institute of Science and Technology, Sao Jose dos Campos, Brazil

ARTICLE INFO

Keywords:
Interlaminar fracture toughness
Thermoplastic composites
Buckypapers
Fractography

ABSTRACT

Carbon fiber reinforced polymer (CFRP) composites are widely used to produce structural components. However, their low interlaminar strength makes them susceptible to delamination, limiting structural applications. Aiming to solve this problem, this work proposes adding carbon nanotubes buckypaper (BP) into CFR thermoplastic composites as an interlayer to enhance the interlaminar strength through the BP bridging effect. Despite this objective, the carbon nanotube BP changed the delamination behavior in mode-I, creating an easy pathway for crack growth (smooth fracture surface) and reducing the interlaminar strength. An opposite behavior was observed for mode-II, in which BP acted as an obstacle for crack growth through the shear direction due BP bridging effect, which slightly improved interlaminar strength, resulting in a rougher surface. The experiments demonstrated through the energy involved in crack growth, the roughness of the fracture surface, and the amount of fracture mechanisms when BP was incorporated that in mode-I the delamination strength decreased, while it increased under the shear mode. This evidences that the BP bridging effect is influenced by the loading mode. Finally, this work highlights the need to study individual modes I and II in composites with buckypaper as an interlayer, since it influences the interlaminar toughness differently.

1. Introduction

Carbon fiber reinforced polymer (CFRP) composites are widely used as structural components in the aerospace industry, especially in applications that require weight reduction and high performance [1]. Among the CFRP applications, thermoset polymers demand the highest revenue, as cited by the AVK report [2]. However, thermoplastic matrices represented 28.8 % of the investments in CFRP in 2018, evidencing its growth and high market demands [2]. Thermoplastic composites are notable for their high stiffness and specific strength, besides the quick manufacturing process (compared to thermoset composites), recyclability, improved fracture toughness, higher chemical and environmental resistance, superior impact performance, good tolerance to damage, and the components joining through welding techniques [3,4]. Therefore, fiber-reinforced thermoplastic composites have attracted special attention in both academic and industrial fields, revealing promising applications as structural materials and a substitute for thermosets composites.

The low interlaminar strength of the CFRP makes them susceptible to delamination, limiting its application in engineering areas [5]. Delamination consists of ply decohesion of laminated composite, occurring under tensile peel loading (mode-I), shear loading (mode-II) or a combination of both (mixed mode). This failure can easily start due to material defects or impacted fracture damage, thus generating stress concentrations [6]. Therefore, an improvement in the interlaminar strength can result in better damage resistance and, consequently, an increase in the performance and durability of the material. Over the last few years, researchers have studied new methods to improve interlaminar fracture toughness. Among the available procedures, the incorporation of nanofillers stands out for increasing the toughness of the matrix. Also, add multifunctionality to the composite enabling better thermal and electrical properties [7].

In this context, nanostructured polymer composites based on the addition of carbon nanotubes (CNT) have been of great importance to

* Corresponding author.
E-mail address: luis.santos@unesp.br (L.F. de Paula Santos).

https://doi.org/10.1016/j.compstruct.2023.117507
Received 10 March 2023; Received in revised form 18 July 2023; Accepted 23 August 2023
Available online 24 August 2023

the scientific community, mainly due to their excellent mechanical, electrical, and thermal properties, as well as their low specific weight (1.0 – 2.0 $g.cm^{-3}$) [8–11]. One of the challenges to CNT composite structures lies in obtaining an adequate dispersion of the nanofiller, due to the van der Waals forces between the tubes, resulting in non-homogeneous materials [12,13]. Carbon nanotube films (buckypapers – BP) come as an alternative for preparing nanostructured polymer composites, as considered by researchers [14,15]. BP is a porous film formed by a highly dense structure of CNTs cohesively bonded by van der Waals forces. The CNT film is commonly obtained by vacuum filtration of a CNT suspension randomly distributed [16,17].

Some studies reported in literature demonstrate the efficiency of BP composites in preventing the delamination of composite materials. For instance, Liu, Shen, and Zhou [18] showed that adding CNT BPs in the epoxy/carbon fiber composite promoted a 74 % and 82 % improvement in G_{IC} and G_{IIC}, respectively. Also, the inclusion of BP in carbon fiber-reinforced phenolic laminate showed an enhancement of 30 % for interlaminar toughness (mode I), as reported by Chan, Li, and Yu [19]. Shin and Kim [20] studied epoxy reinforced with unidirectional (UD) and woven carbon (WN) fiber interleaved with carbon nanotube buckypapers. The results demonstrated an increase in fracture toughness in mode-I and II. However, the buckypaper affected the material properties differently: for mode-I, the contribution was more significant for WN laminate, whereas for mode-II, the greatest gain was for UD laminate. Therefore, the buckypaper contribution is related to the crack propagation behavior and loading mode.

Yazdanparast and Rafiee [21] studied the effects of pull-out speed on the critical interfacial shear stress (CISS) between CNT and epoxy resin, in which the pull-out mechanism contributes to bridging crack growth. The molecular dynamics (MD) simulation of the optimized unit cells revealed a inverse correlation between the pull-out speed and the maximum pull-out force. Additionally, the CNT length and diameter affect the pull-out speed. Rafiee and Sahrae [22] explained that the experimental data follows the proposed simulation methodology, showing that CNTs prove to be a good alternative. In their work, unidirectional glass fibers/epoxy composites reinforced with CNT were prepared and submitted to mode-I interlaminar fracture test to characterize laminated composites containing CNTs dispersed in the matrix. All the mentioned studies attributed the increase of interlaminar strength to the bridging effect caused by buckypaper. As reported, the CNT film hinders crack growth and shifts the interlaminar toughness to higher values. However, the loading imposed during the test could affect the material behavior and how much the BP bridging will contribute to damage control.

In this work, carbon nanotube buckypapers (BP) were used as interleave for two composite systems, carbon fiber-reinforced poly (ether imide) (PEI) and poly (aryl ether ketone) (PAEK), manufactured by hot compression molding. With that, this work investigated the buckypaper on the interlaminar fracture toughness of the composites. Particularly, a physics-based approach to study quasi-static delamination growth is adopted, enabling careful study of the micro-mechanisms involved. It is important to highlight that three-phase structural composites have not been fully explored, especially those composed by high-performance thermoplastics and carbon nanotube buckypapers. The focus of most works is on three-phase structural composites made by thermoset matrix or two-phase composites (polymer and nanoparticles), aiming to disseminate the knowledge in this field among the scientific community.

2. Experimental procedures

2.1. Materials

Multi-walled carbon nanotubes (MWCNT) were synthesized by chemical vapor deposition (purity > 92 %) and provided by Nanografi, a German company. The MWCNTs were functionalized with a carboxyl group (COOH), showing internal and external diameters of 5–10 nm and 8–15 nm, respectively, and their lengths vary from 1 to 3 μm. Triton X-100 (surfactant) consists of a viscous/colorless liquid with a pH of around 6.0–8.0, a boiling temperature of 200 °C, and a specific mass of 1.07 $g.cm^{-3}$. Poly (ether imide) was supplied by Sabic's Innovative Plastics – Brazilian facility, coded as ULTEM 1000, with the following properties: specific mass of 1.27 $g.cm^{-3}$ and glass transition temperature (T_g) of 217 °C. TC1225 (poly (aryl ether ketone) (PAEK)/carbon fiber) and TC1000 Premium (poly (ether imide) (PEI)/carbon fiber) were supplied by Toray Advanced Composites (Netherlands) and used to produce the laminates.

2.2. Buckypaper fabrication

The buckypaper (BP) was manufactured using the vacuum filtration technique, and the details are provided in an earlier study [23]. To summarize, 50 mg of MWCNT were dispersed in 100 mL of deionized water with 1 g of Triton X-100 on an ultrasonic tip (Hielscher - model UP400st). The MWCNT suspension was centrifuged for 30 min at 4000 rpm and then vacuum filtered in a homemade system with dimensions of (300 × 100) mm, using a nylon membrane (0.45 μm) and PEI mats produced by electrospinning procedure. Polymeric mats were obtained from 15 % w/w PEI solution solubilized in N-methyl-2pyrrolidone/dimethylacetamide (NMP/DMAC) (7:3 by volume) using a magnetic stirrer at 60 °C. The parameters used to produce the PEI mats were cylinder rotation of 60 rpm, stainless steel needle of 2 mm in diameter and 8 mm long, voltage of 19 kV, working distance of approximately 8 mm, temperature of 21 °C, and time collection of 3 h. PEI/mats were produced with a thickness of 40 μm and used as substrate during the BP filtration step. Subsequently, BP was dried in a vacuum oven at a temperature of 100 °C for 8 h. The average thickness of the BP/PEI mats was 66 μm and 88 μm for PEI/CF/BP and PAEK/CF/BP, respectively. Thickness difference is due to pressure applied to each composite during the processing. Moreover, it is worth noting that the use of BP with PEI mats was based on a previously published article that showed better properties compared to BP [23].

2.3. Composite processing and characterization

Buckypaper carbon fiber-reinforced polymer composites (PEI and PAEK) were processed using 16 layers of semipregs. The stack sequence was $[(0/90)]_{8s}$ and a BP/PEI mat was placed at the mid-plane of the laminate. The pre-crack was introduced by one layer of polyimide film with a thickness of 0.13 μm in the laminate mid-plane. The composites were consolidated in a hydraulic press. The processing parameters for PAEK composites started heating the material to 350 °C, followed by a 30-minute threshold to reach the temperature homogenization. Subsequently, a pressure of 1 MPa was applied (maintained until the end of the processing) and after 20 min the material was cooled to room temperature. The same parameters were used for PEI composites, except for the pressure, which was 2 MPa. The laminate dimensions were (500 × 500 × 4.8) mm. Four configurations were processed, following the base material for comparative analysis – PAEK/CF and PEI/CF. The content of carbon nanotubes for each nanocomposite was 3.0 wt%.

2.4. Sample preparation

After processing steps, the laminates were cut using a Proth cutting grinding machine equipped with a diamond disc. The geometry and dimensions of the specimens were based on the ASTM D 5528-12 for DCB tests [24] and ASTM D7905-14 for ENF tests [25]. The dimensions for each test specimen are shown in Fig. 1. One side of the specimens was carefully sanded and coated with white paint to visualize the crack tip, and a ruler was also bonded to help estimate the crack length. Also, an aluminum block was attached at both surface edges of the specimen submitted to DCB tests, as illustrated in Fig. 1a.

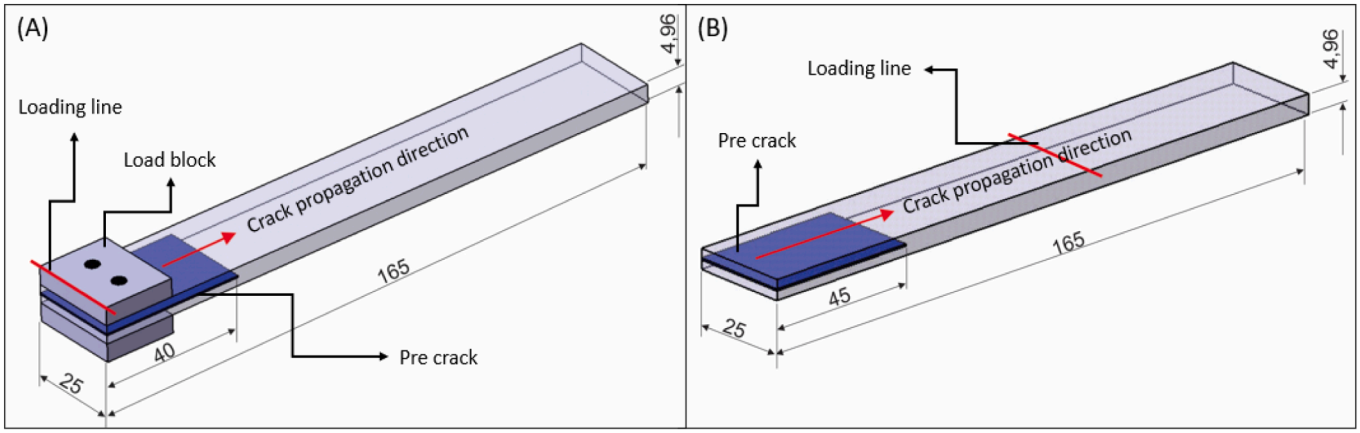

Fig. 1. Geometry and dimensions of the samples for (A) DCB and (B) ENF tests.

2.5. Quasi-static tests

The mode-I and mode-II fracture behavior for all processed laminates were performed through a double cantilever beam (DCB) according to ASTM D5528-13 [24], and end-notched flexure (ENF) tests following ASTM 7905-14 [25]. DCB and ENF tests were performed in an MTS machine with a 10 kN load cell and a high-resolution camera was used to monitor the crack propagation. The setups configuration used to perform the DCB and ENF tests are presented in Fig. 2. The experiments were conducted under displacement control using a speed rate of 1 mm/min. Opening displacement (δ) was applied to the sample until the crack achieved a length of 100 mm for the DCB test. For the ENF test, the displacement was applied until reaching the maximum load, and a constant drop was observed. Five samples of each condition were used for quasi-static tests under mode-I and mode-II. Mode-I interlaminar fracture toughness (G_{IC}) was calculated using the Compliance Calibration (CC) method, as described [24]:

$$G_{IC} = \frac{nP\delta}{2ba} \tag{1}$$

where P is the load, δ is the displacement, b is the width, a is the crack length, and the exponent n is obtained from the slope of the graph a versus C *(compliance* – δ_i/P_i*)*.

Mode-II interlaminar fracture toughness (G_{IIC}) was calculated based on [26] according to equation (2), which corresponds to the classical theory beam–load deflection method.

$$G_{IIC} = \frac{9Pa^2\delta_d}{2B(2L^3 + 3a^3)} \tag{2}$$

Where P is the load, a is the crack length, δ_d is the displacement, B is the sample width, and L is half of the span length.

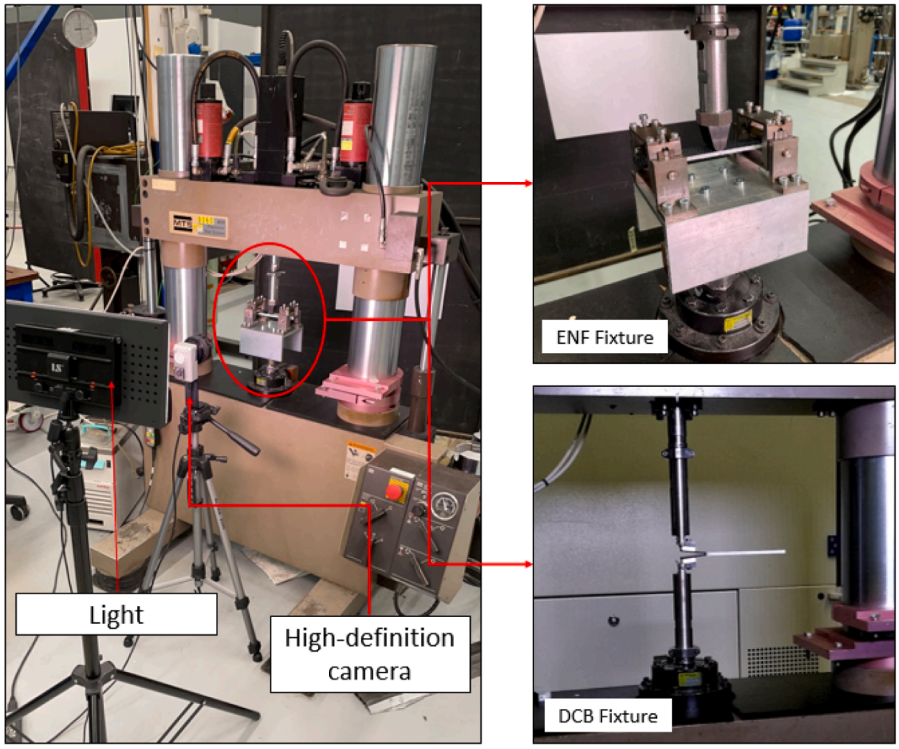

Fig. 2. Setup configuration for DCB and ENF under quasi-static conditions.

2.6. Energy calculation from Quasi-static data

According to Griffith [27], the crack growth process involves the creation of new surfaces, which requires energy to dissipate. Therefore, it is essential to understand the differences in released energy involved in both load conditions and which mechanisms generated such differences. For this reason, the quasi-static data (mode-I and mode-II) were also used to calculate the energy involved in crack growth according to the method presented on ASTM D5528, Amaral et al. [628] and Alderliesten [29]. Therefore, the data was discretized to calculate *dU/dN* (U is the energy) and *da/dN* (a is the crack length), considering the energy recovery after a crack increment as a cycle. In this work, the quasi-static data were discretized in four different levels (steps), previously proposed by Amaral et al. [6], as schematically illustrated in Fig. 3. Fig. 3a represents the first step corresponding to the observed crack growth during the test. Subsequently, the *dU* of the same crack was calculated, considered half *da* (Fig. 3b), one and a half (Fig. 3c), and two of the observed *da* (Fig. 3d). It is important to point out that the crack measurement data remains the same, but it was discretized at different levels. Also, the fracture surface and the energy involved in creating the fracture surface were not affected by this procedure.

2.7. Fractographic analysis

Fracture surfaces of the samples submitted to mode-I and mode-II tests were analyzed using an optical microscope (Keyence VR-5000 wide-area 3D measuring system) and a scanning electron microscope – SEM (JEOL JSM-840 EDS). The optical microscope was used to analyze the fracture surface quantitatively. Thus, a length of 30 mm after the pre-crack was considered. In this case, the fracture surface was cleaned with a nitrogen jet, and no sample preparation was carried out to avoid any change in fracture patterns. The focus variation microscopy was used, which the image is obtained from the movement of the lens vertically in relation to the objective, resulting the object in and out of focus. The sensors of the microscope detect and measure in-focus pixels, building an in-focus image from the vertical scan. Thus, the surface topography and roughness are calculated through the in-focus depth of each plane and an image from the in-focus slices is obtained [30]. The arithmetical mean (S_a), where the height difference of each point is compared to the arithmetical mean, of the fracture surface was calculated as follows:

$$S_a = \frac{1}{A}\int_A^n \int |Z(x,y)|dxdy \tag{6}$$

The SEM analysis was performed to evaluate the mechanisms presented at the fracture surface after the mechanical tests. For this analysis, the specimens were cleaned with a nitrogen jet and sputter-coated with gold to provide good electrical conductivity. The parameters used were a work distance of approximately 10 mm and a probe current of 5 kV.

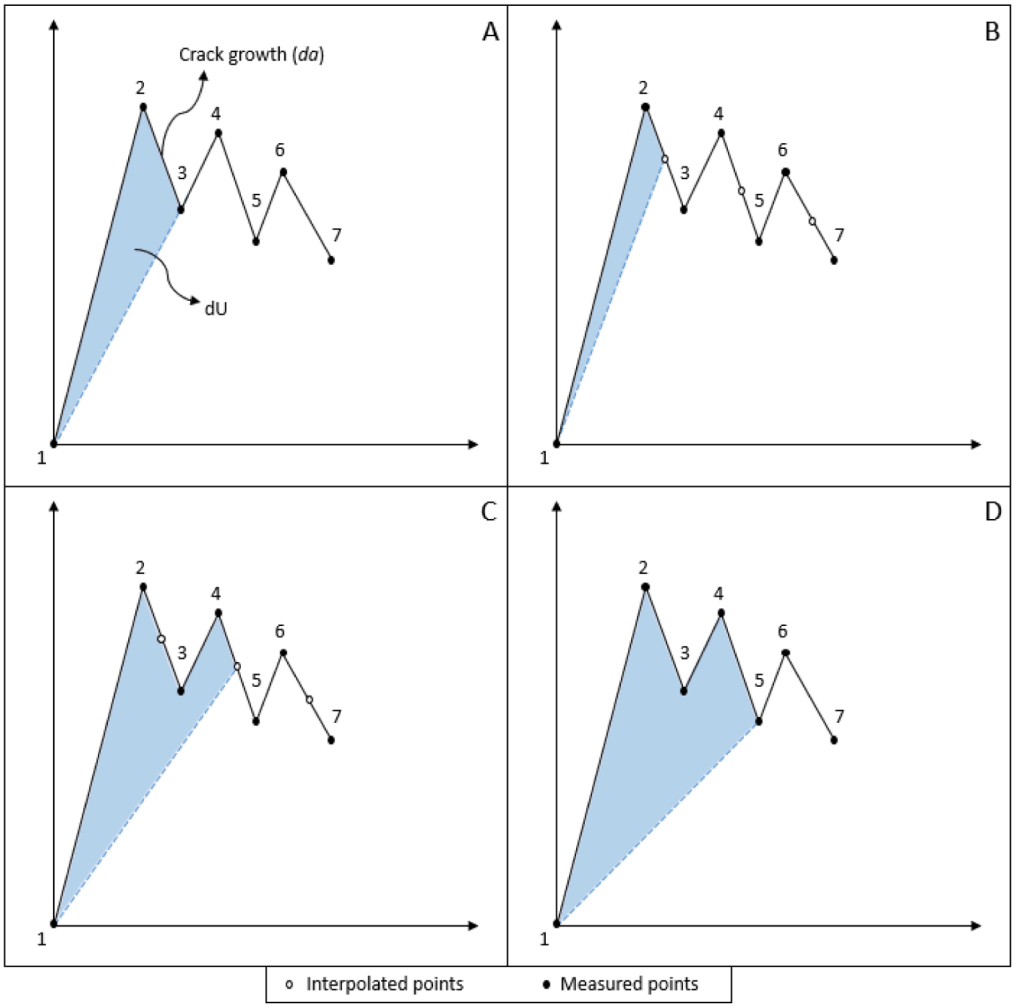

Fig. 3. Scheme of how quasi-static data was used to obtain dU/dN and da/dN from mode-I and mode-II tests(a) observed crack growth, (b) half, (c) one and half, and two of the observed crack growth (da).

3. Results and discussion

3.1. Interlaminar toughness under mode-I

A typical load–displacement curve and R-curves (G_{IC} versus crack length) obtained from the DCB test for all laminates are shown in Fig. 4 and Fig. 5, respectively. By analyzing the load–displacement curves in Fig. 4A and 4C, it is observed that base laminates (PAEK/CF and PEI/CF) presented a linear behavior during the initial phase associated with elastic behavior from linear fracture mechanics. Subsequently, a drastic drop in force is reported, followed by an increase and subsequence drop during the test according to crack growth and stiffness change. This behavior is related to the unstable crack propagation called stick–slip, which is observed 4 to 6 times per sample. Regarding R-curves (Fig. 5A and 5C) even with some scatters in the values, the interlaminar toughness remains almost constant during the test.

Similar behavior was found for BP/PEI mats (PAEK/BP/CF and PEI/BP/CF) laminates. Nevertheless, the force and displacement applied during the test are inferior to PAEK/CF and PEI/CF, as shown in Fig. 4B and 4D. Also, the R-curves (Fig. 5B and D) for both laminates showed a larger scatter with reduced fracture toughness. The average interlaminar toughness (G_{IC}) was calculated using the load, displacement, and crack length values before the unstable crack propagation. The G_{IC} values are presented in Table 1.

The G_{IC} results showed that adding BP/PEI mats negatively affected this property, reducing approximately 68 % and 80 % for PAEK and PEI/CF, respectively. In addition, a higher deviation was observed for those materials with buckypaper, mainly PEI/BP/CF. The explanation of such reduction will be presented later in this section with the assistance of microscopy images. As aforementioned, energy is required for the occurrence of crack propagation, and this process creates new fracture surfaces [26,31]. Therefore, microscopy analyses were performed to understand the contribution of BP/PEI mat.

The fracture surfaces of the composites were initially evaluated using an optical microscope, and the fractured surface roughness was analyzed. The images are shown in Fig. 6. The pre-crack is the brighter area on the left side, which was not considered during the roughness analysis.

PAEK/CF and PEI/CF presented similar fracture surfaces in the mode-I test, in which the average roughness (S_a) results were 89.95 ± 0.278 μm and 66.92 ± 0.171 μm, respectively. The laminates were processed using woven carbon fiber, so it is possible to observe the weft and warp, besides the matrix on the fracture surface of the base laminates. PAEK/CF/BP and PEI/CF/BP laminates presented CNT films on both fracture surfaces, indicating that the crack had propagated inside the buckypaper. Also, the average roughness for BP laminates is 67.58 ± 0.299 μm (PAEK/CF/BP) and 41.72 ± 0.379 μm (PEI/CF/BP), a respective reduction of 25 and 38 %. Adding buckypapers reduced the

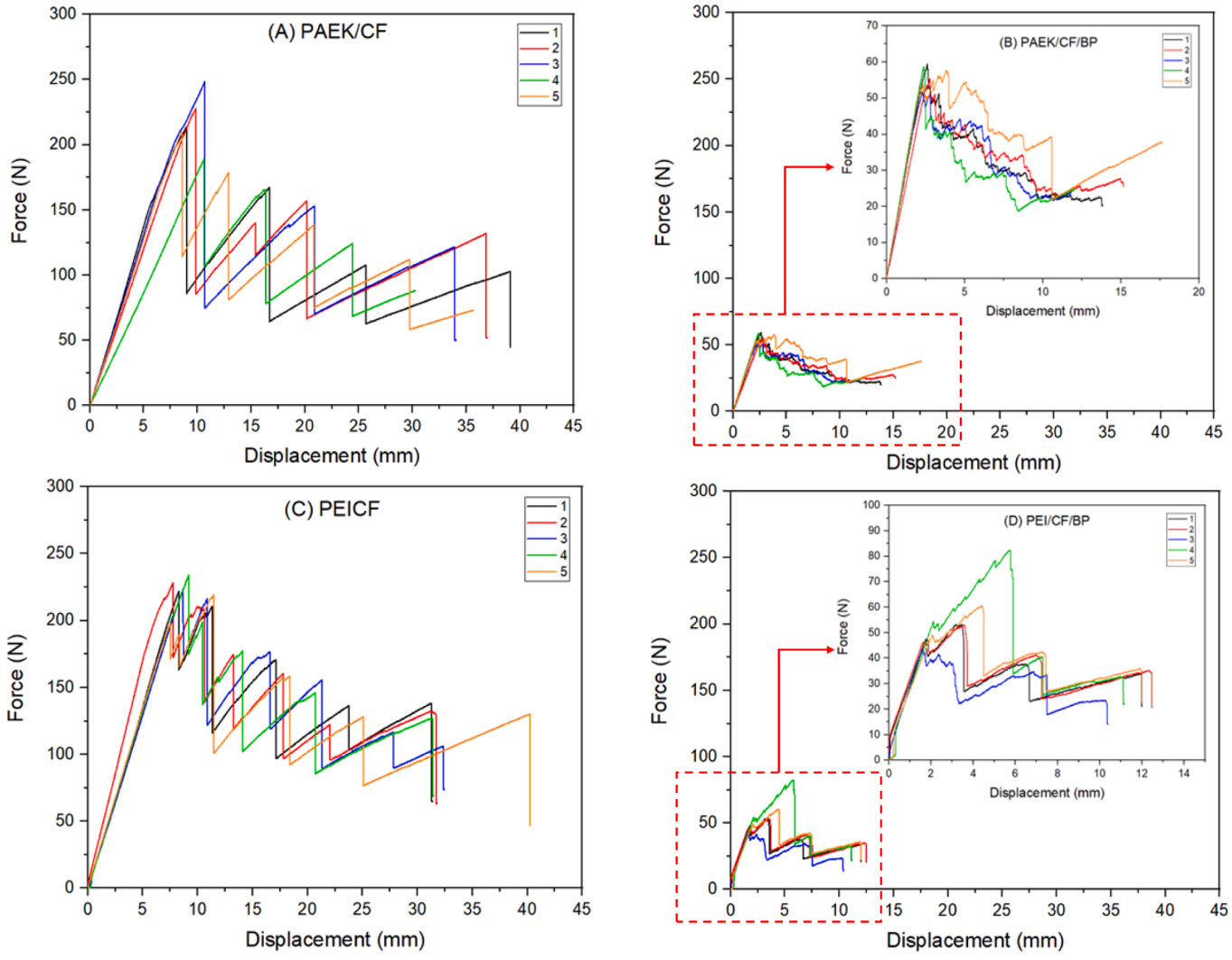

Fig. 4. Load-displacement curves obtained via DCB (mode-I) test for (A) PAEK/CF, (B) PAEK/BP/CF, (C) PEI/CF, and (D) PEI/BP/CF laminates.

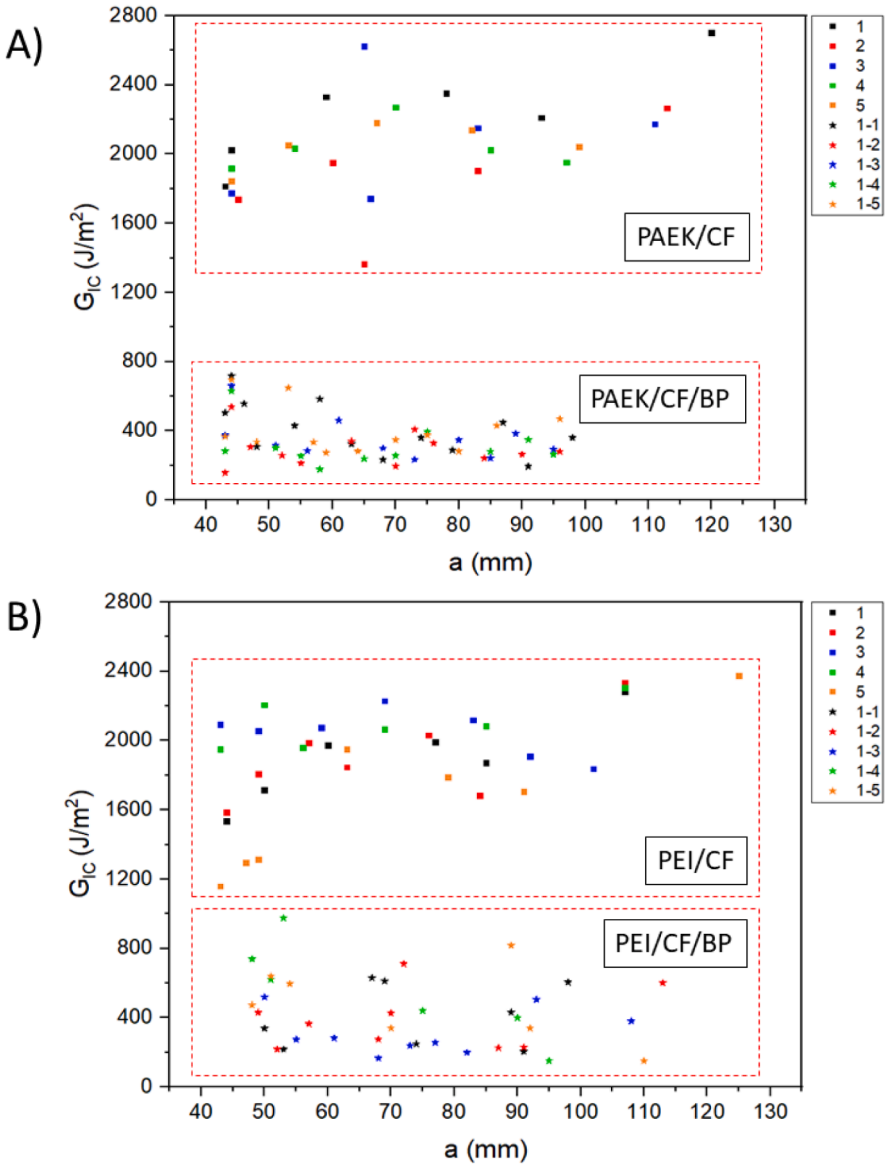

Fig. 5. R-curve (G_{IC} versus crack length) under mode-I conditions for (A) PAEK/CF and PAEK/BP/CF, and (B) PEI/CF and PEI/BP/CF laminates.

Table 1
Mode-I Interlaminar fracture toughness (G_{IC}) for all laminates studied.

Specimen	G_{IC} (J/m²)			
	PAEK/CF	PAEK/CF/BP	PEI/CF	PEI/CF/BP
1	2239.16	717.61	1895.87	224.37
2	1844.88	537.83	1896.90	232.22
3	2093.42	660.03	2046.21	297.35
4	2039.89	630.37	1739.40	453.00
5	2052.06	695.92	1655.15	312.03
Average	2053.9	648.35	1846.70	303.79
SD	126.31	62.82	136.34	82.22
CV (%)	6.15	9.69	7.38	27.06

* *SD* – Standard *deviation / CV – Coefficient of variation.*

surface roughness, suggesting reduced mechanical anchoring and lower energy required for crack propagation. According to Amaral et al. [6], the lower energy required for crack propagation is reflected in the surface roughness, confirming the results found. As can be noted, smoother surfaces require lower strain energy due to lower interlaminar resistance in mode-I. In addition, PAEK/BP/CF and PEI/BP/CF presented only flaws of the matrix on their surface, indicating that weft and warp were overlaid by the BP layer, which reveals low transverse strength.

To better visualize the mechanisms involved in the crack propagation for all laminates, SEM analysis was performed, as shown in Figs. 7 and 8. The fracture surface for the base laminates has ordinary aspects of mode-I fracture patterns, such as broken fibers (blue arrows), matrix cleavage (green arrows), cusps (red arrows), and fiber imprints (orange arrows) [6,32,33]. The fracture surface for PAEK/CF presented higher roughness than PEI/CF, which suggests that higher energy is involved in crack growth. This fact agrees with the results obtained for G_{IC} values, R-curves, and roughness for PAEK/CF and PEI/CF composites.

According to the literature [7,26,34], carbon nanotubes generally increase interlaminar toughness. This behavior is due to the nanofillers trend to increase the surface area of the crack tip, acting as a bridge, increasing the energy involved in the crack growth and, thus the interlaminar toughness. However, the carbon nanotube buckypapers promoted a decrease in the interlaminar toughness for mode-I. The fracture surface for PAEK/CF/BP and PEI/CF/BP presented in Fig. 8 reveals that the fracture surfaces have matrix-related failures, such as river lines (yellow arrows). With higher magnification (× 15k), it was possible to observe the carbon nanotubes on these surfaces. Features such as broken

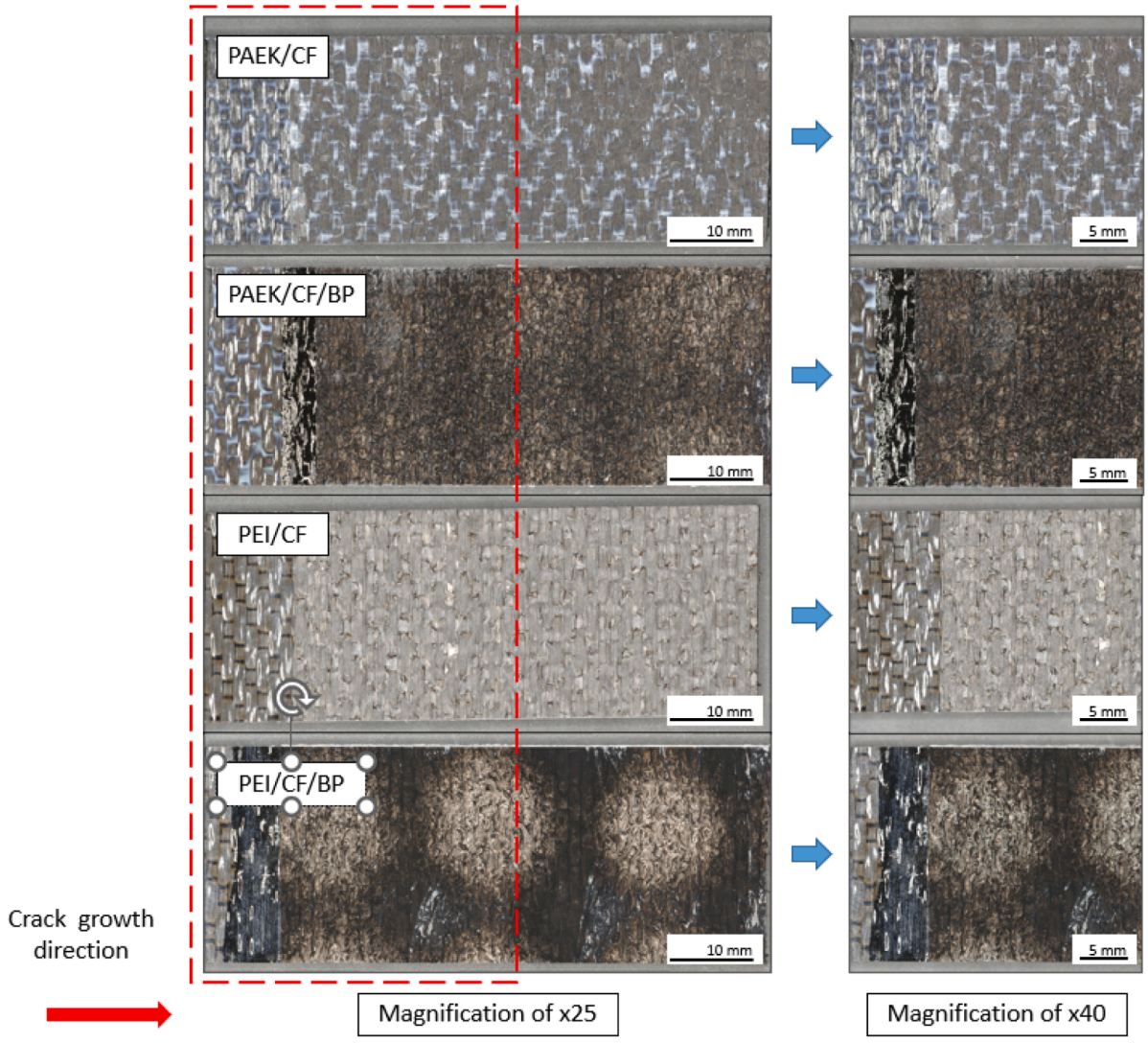

Fig. 6. Optical microscopy images of the mode-I fracture surfaces for all samples.

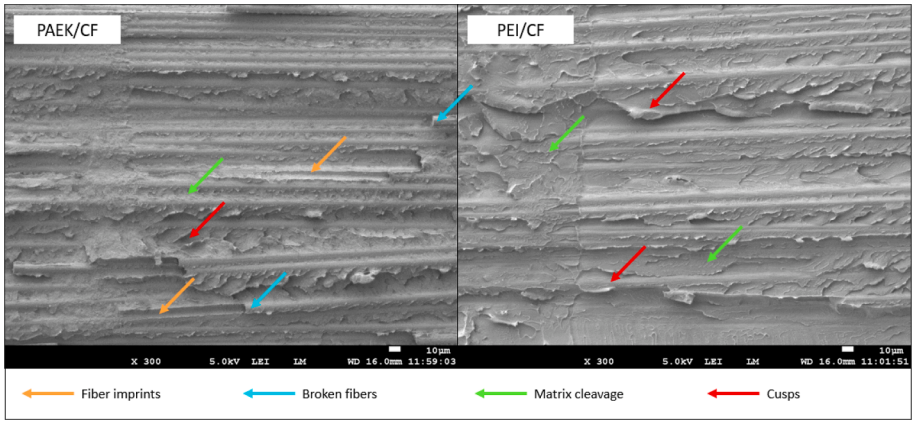

Fig. 7. SEM micrographs of the mode-I fracture surface for PAEK/CF and PEI/CF. The mechanisms observed are broken fibers (blue arrows), matrix cleavage (green arrows), cusps (red arrows), and fiber imprints (orange arrows). (For interpretation of the references to colour in this figure legend, the reader is referred to the web version of this article.)

fibers and fiber imprint were not observed for these laminates, indicating that the crack propagates inside de buckypaper/PEI mats layer.

According to Amaral et al. [6], the amount of damage generated during the experiment relates to the energy released during crack growth per unit area. Decohesion failure involves breaking chemical bonds to propagate the crack, and if more decohesion happened, more

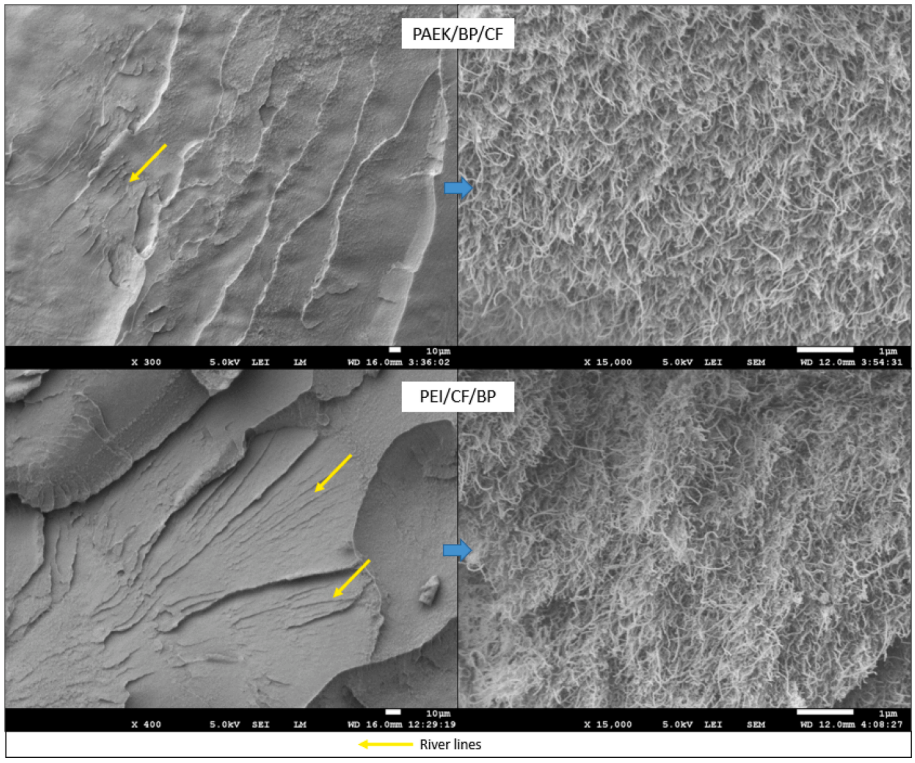

Fig. 8. SEM micrographs of the mode-I fracture surface for PAEK and PEI/BP/CF with river lines (yellow arrows) along the surface. (For interpretation of the references to colour in this figure legend, the reader is referred to the web version of this article.)

energy was released per unit area. The difference in the damage state gives information about the amount of energy dissipated during crack growth, making it easy to understand the effect of carbon nanotube buckypapers on the interlaminar toughness. The data from the quasi-static test were used to calculate the energy involved in crack growth, as described in *Section 2.6*. The results obtained are presented in Fig. 9 and summarized in Table 2. From the average values of *dU/dN* and *da/dN* trendlines were obtained, of which the slopes indicate the

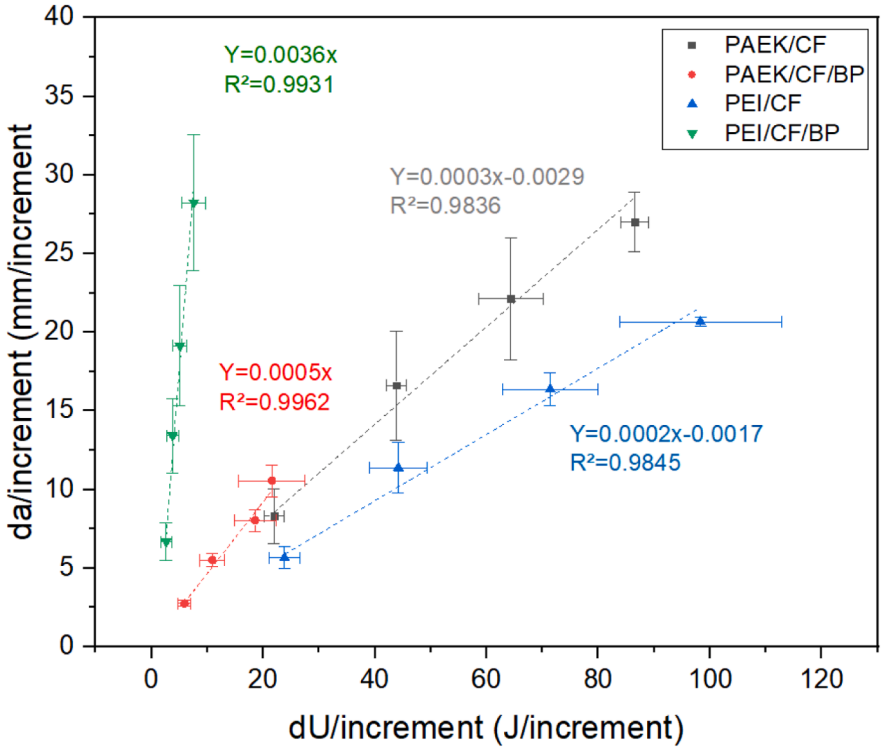

Fig. 9. Average values of dU/increment versus da/increment obtained from quasi-static data for all laminates under mode-I at four different levels.

Table 2
Average values for dU/increment and da/increment obtained from mode-I quasi-static data at four different levels.

Samples	Average Values							
	1st set		2nd set		3rd set		4th set	
	dU*	da**	dU*	da**	dU*	da**	dU*	da**
PAEK/CF	21.94	8.3	43.85	16.6	64.34	22.1	86.52	27.0
PAEK/CF/BP	5.93	2.7	10.89	5.5	18.58	8.0	21.58	10.5
PEI/CF	23.85	5.6	44.21	11.3	71.39	16.3	98.28	20.6
PEI/CF/BP	2.65	6.6	3.79	13.4	5.11	19.1	7.59	28.2

* dU/increment (J/increment) / **da/increment (mm/increment).

interlaminar resistance and the energy dissipated in crack growth, enabling comparison with fracture surface behavior. In other words, a lower slope represents complex damage features (rougher surface with more damage features), requiring more energy for delamination [35], and the opposite is observed for a steeper slope. The results (Fig. 9) showed a good linear fit and coefficient of determination ($R^2 > 0.97$).

The resistance to mode-I delamination growth (defined by slopes) ranks in the following order: PEI/CF > PEAK/CF > PEAK/CF/BP > PEI/CF/BP. The BP layer imposed a higher decrease in interlaminar resistance between PEI/CF and PEI/CF/BP (i.e., 205 % of reduction) than between PEAK/CF and PEAK/CF/BP (i.e., 66 % of reduction). From obtained data of dU/dN and da/dN the buckypaper laminates present low strain energy compared to those without buckypaper, confirming the previous analysis.

For mode-I, the carbon nanotube buckypaper created an easy pathway to crack growth, reducing the interlaminar toughness and the required strain energy. The mechanical properties of nanostructured composites are extremely dependent on the interfacial strength, which determines the effectiveness of load transfer across the interface [36]. Generally, carbon nanotubes and matrices tend to interact by covalent or electrostatic interactions, π-stacking, or hydrogen bonds which are strong interactions compared to van der Waals forces [36]. As observed, the PAEK/CF/BP and PEI/CF/BP presented buckypaper in both fracture surfaces (top and bottom sides), suggesting that the crack propagates inside the buckypapers. This behavior can be attributed to the matrix squeeze inside the buckypaper generated during the hot compression molding. It is noteworthy that pressure applied during the manufacture step it is higher for thermoplastic than thermoset composites. The "dry area" inside the buckypaper composed of carbon nanotubes cohesively bonded by van der Waals forces is weaker than the strong bonds presented by the BP/matrix interface, reducing the energy for crack growth. Since this region is the weakest, the crack growth remained inside the BP/PEI mat, as schematically illustrated in Fig. 15A. In addition, the crack propagates very straight during the test, as shown in Fig. 15B, which contrasts with literature works [27,34] that observed an angle of approximately –45°. The data presented showed that carbon nanotubes did not act as a bridge, hindering crack growth and dissipating more energy by creating an easy pathway for crack growth.

3.2. Interlaminar toughness under mode-II

The interlaminar toughness under shear loading (mode-II) was studied with the ENF experiments. The load–displacement curves obtained during the test are shown in Fig. 11. All laminates had similar behavior when submitted to the shear test. In other words, they all initially possess a linear segment related to the stable crack propagation followed by a force drop due to unstable crack propagation. The interlaminar fracture toughness (G_{IIC}) was calculated using the load and displacement at crack initiation, as shown in Table 3. In this case, BP/PEI mat promoted an increase in interlaminar toughness. PAEK/CF/BP showed an improvement of 8.87 % in fracture toughness G_{IIC} compared with PEAK/CF. The same trend was observed for PEI composites, in which PEI/CF/BP exhibited an enhanced G_{IIC} of 4.81 % compared to the base laminate.

The microscopic images of fractured surfaces are presented in Fig. 12. PAEK/CF and PEI/CF showed similar results, whereas PAEK/CF/BP and PEI/CF/BP revealed different aspects of the fracture surface. It is noted the amount of the carbon nanotube film is higher at the end of the crack propagation, in other words, the crack becomes to drag the film as it propagates in the laminate, remaining a higher amount of carbon nanotube film at the end of the crack. Initially, the surface roughness was measured through optical microscopy of the region analyzed which is highlighted by a red rectangle (dash line) in Fig. 12. The roughness results were 68.29 ± 0.406 μm (PEAK/CF), 84.78 ± 0.397 μm (PEI/CF), 130.71 ± 0.327 μm (PEAK/CF/BP), and 92.02 ± 0.382 μm (PEI/BP/CF). The measured roughness results follow the G_{IIC} values, in which the materials with BP/polymeric mats presented higher values than standard materials (PAEK/CF and PEI/CF).

PAEK/CF and PEI/CF composites had typical and similar fracture surfaces in which the main features observed are fiber imprints, cusps, matrix cracking, and some debris. Plastic deformations at the fiber imprint edges are also visible in some regions. The features (Fig. 13)

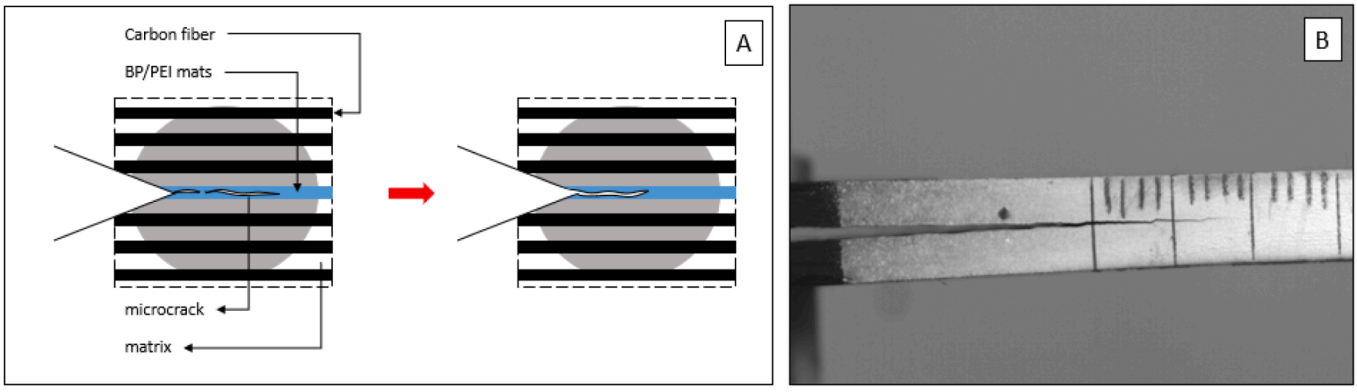

Fig. 10. (A) Scheme of the crack formation and its propagations for PAEK/BP/CF and PEI/BP/CF, and (B) real example of initial straight crack propagation observed during the test.

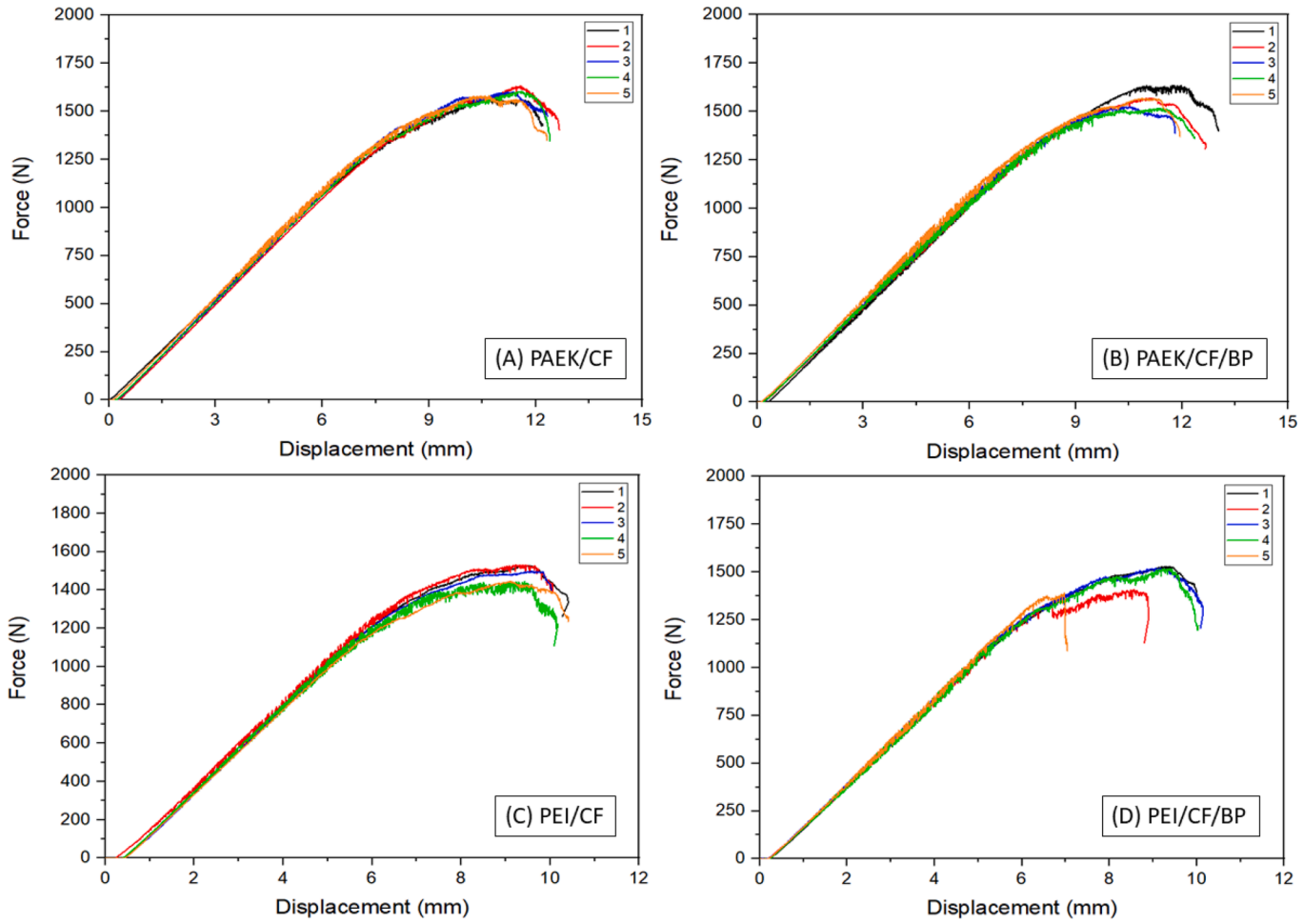

Fig. 11. Load-displacement curves obtained via ENF (mode-II) test for PAEK/CF, PAEK/BP/CF, PEI/CF, and PEI/BP/CF laminates.

Table 3
Mode-II interlaminar fracture toughness (G_{IIC}) for all laminates studied.

Sample	G_{IIC} (J/m^2)			
	PAEK/CF	PAEK/BP/CF	PEI/CF	PEI/BP/CF
1	2740.14	2984.52	2583.89	2521.31
2	2697.14	3110.43	2021.75	2446.92
3	2770.82	2754.44	2215.55	2449.41
4	3087.84	3044.22	2265.67	2709.00
5	2781.03	2832.87	2676.52	2202.33
Average	2815.39	2945.30	2352.68	2465.79
SD	139.31	132.41	242.58	162.65
CV (%)	4.95	4.49	10.31	6.59

* *SD – Standard deviation; CV – coefficient of* variation.

observed in each surface subjected to the mode-II test are due to adhesive failures (matrix/fiber interface) and matrix decohesion [28,32,37].

The incorporation of buckypaper as interleaving changed the mode-II fracture surface, as shown in Fig. 14. SEM images revealed that the fracture surface of BP composites presented higher roughness than base laminates. PAEK/CF/BP showed debris, fiber imprints, and cusps patterns. Also, debris of buckypaper was observed. In this case, the plastic deformation was more severe than PAEK/CF. PEI/CF/BP showed shear cusps and plastic deformation of the matrix, besides fibers imprint.

The quasi-static data from the shear delamination mode were used to calculate the energy related to the crack growth. For the mode-II test, the data were discretized in different steps described in *Section 2.6*. The obtained results are shown in Table 4 and illustrated in Fig. 15. The trendline obtained through linear regression fits the data with $R^2 < 0.99$.

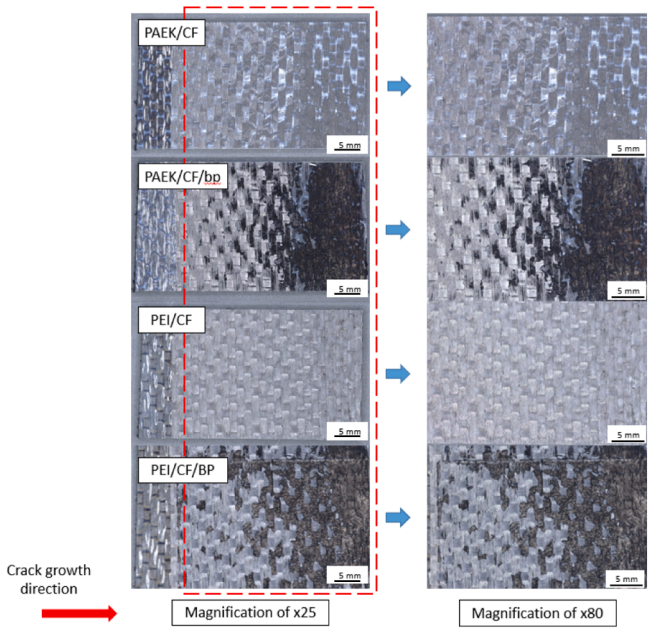

Fig. 12. Optical microscopy images of the fracture surface for samples submitted to the ENF tests.

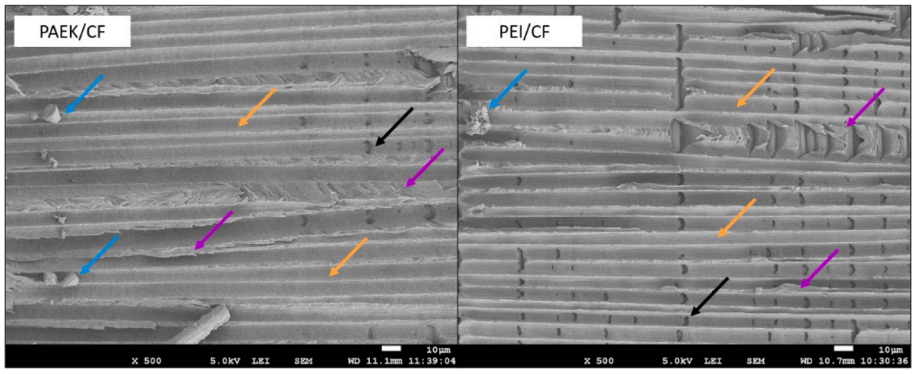

Fig. 13. SEM micrographs of the mode-II fracture surface for PAEK/CF and PEI/CF showing debris (blue arrows), cusps (purple arrows), fiber imprints (orange arrows), and matrix cracking (black arrows). (For interpretation of the references to colour in this figure legend, the reader is referred to the web version of this article.)

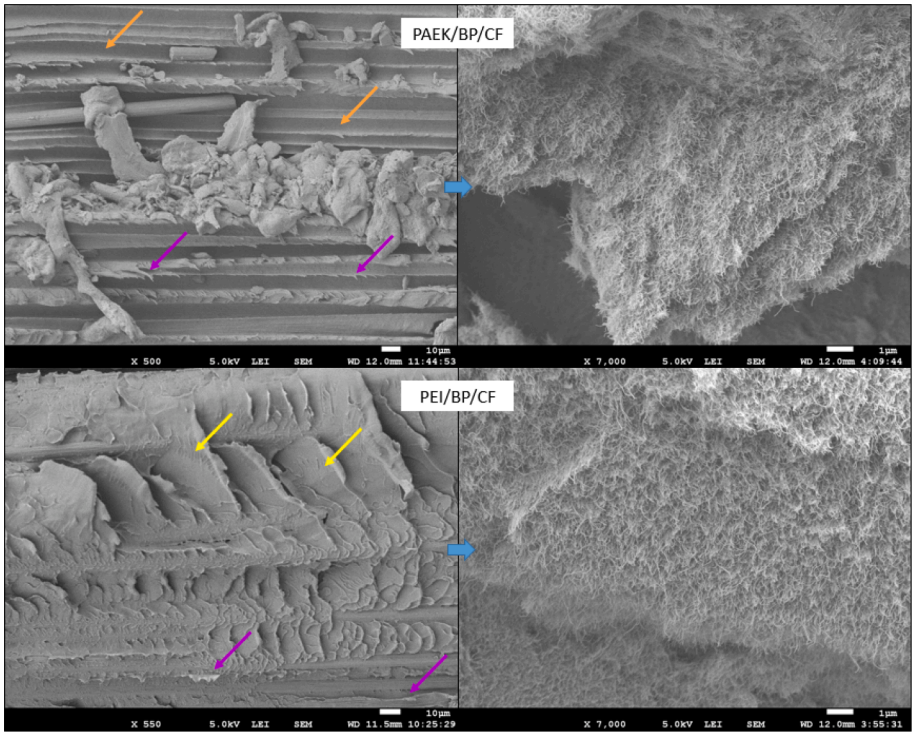

Fig. 14. SEM micrographs of the mode-II fracture surface for PAEK and PEI/BP/CF.

The energy involved in crack growth in the laminates with and without buckypaper is similar, presenting a slight improvement. High energy and crack length were observed for PAEK/CF/BP and PEI/CF/BP composites compared to the base laminates. Also, the fracture surface of BP composites presented a rougher surface with more damage features. The curve slopes follow the sequence: PEAK/CF/BP > PEAK/CF > PEI/CF/BP > PEI/CF.

Quasi-static delamination is generally expressed as fracture toughness as function of strain energy release rate (SERR). The onset value precedes crack growth, which means that it represents a threshold (like stiction in physics) rather than resistance (friction). In addition, this onset fracture toughness is generally higher for mode-II than mode-I, as reported in literature and observed in this work. These higher values for mode-II can be explained by that the method to determine the SERR does not consider the energy dissipation through plasticity and micro-cracking in the process zone ahead of the crack tip. For example, Amaral et al [6], have illustrated that for mode-II, micro-shear cracking occurs ahead in the process zone, which after 'onset' links up. Hence, the mode-II onset fracture toughness intrinsically exhibits energy dissipation through fracture, which mode-I only experiences after onset.

Analyzing the standard onset fracture toughness obtained from DCB (stiction only) and ENF (stiction + friction) tests, the standard laminates (PAEK/CF and PEI/CF) have resistance in the same order of magnitude. Quasi-static data showed that buckypapers affected the initiation threshold with the standard fracture toughness ($G = dU/da$ for $a = 0$). For mode-I delamination, the buckypaper reduced 4 times the onset energy for crack growth for both materials (PAEK/CF/BP and PEI/CF/BP). On the other hand, the buckypaper shifted the onset energy for crack growth to high values for mode-II delamination, since shear cracking is obstructed by the bridging effect of buckypaper, resulting in higher onset energy for crack growth.

Another important aspect is that according to literature [31,38,39], the process zone shape ahead of de crack tip plays a crucial role in crack growth. To capture that influence, determining the strain energy density (SED) helps to understand the experimental observations. For example, the SED for the very first microscopic crack onset is equal for any loading

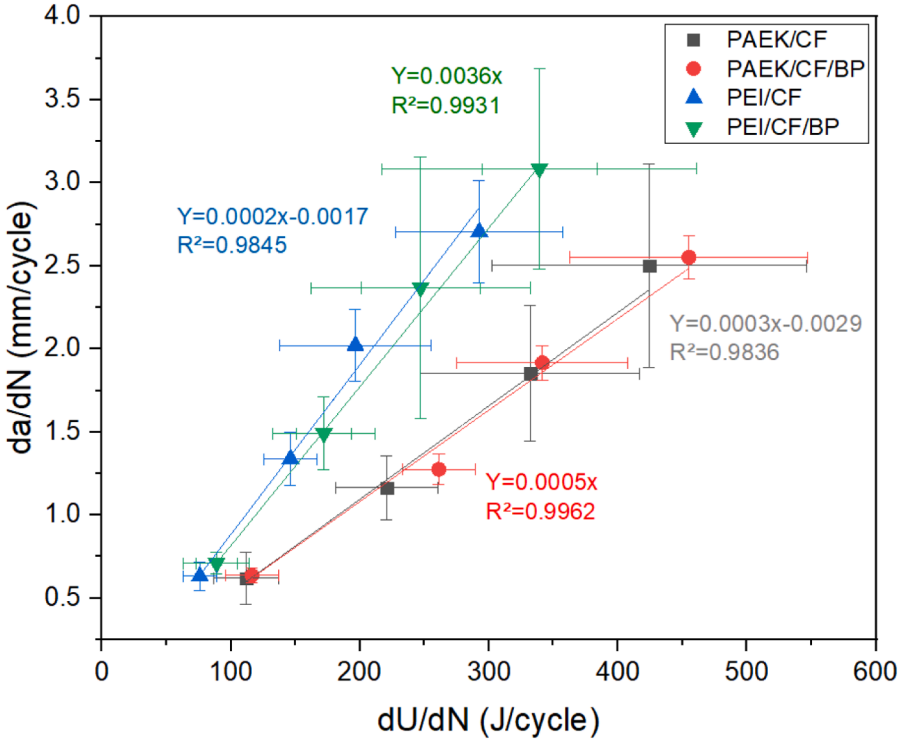

Fig. 15. dU/increment versus da/increment obtained from quasi-static for all laminates under mode-II.

Table 4
Average values for dU/increment and da/increment obtained from mode-II quasi-static data.

Samples	Average Values							
	1st set		2nd set		3rd set		4th set	
	dU*	da**	dU*	da**	dU*	da**	dU*	da**
PAEK/CF	111.85	0.6	220.75	1.1	331.95	1.8	424.16	2.5
PAEK/BP/CF	116.32	0.6	261.21	1.2	341.43	1.9	455.04	2.5
PEI/CF	76.05	0.6	146.24	1.3	196.60	2.0	292.58	2.7
PEI/BP/CF	88.94	0.7	172.12	1.4	247.05	2.3	339.20	3.1

* dU/increment (J/increment) / **da/increment (mm/increment).

mode (I and II) [40]. Beyond that point, a mode-I crack develops a small process zone confined to a crack tip towards crack growth resulting in a straight crack growth (Fig. 10b), while for mode-II a long-elongated process zone develops comprising multiple shear cracks which at 'crack onset' are observed to link-up (Fig. 16b). Hence, in mode-I the onset fracture toughness comprises only storing strain energy prior to crack growth (like stiction in physics), while for mode-II energy is already dissipated through developing shear cracks (additional friction).

Only evaluation the macroscopic response of delamination growth favors overestimation of G_{IC} and G_{IIC} and introduces conservatism during the design of a part or component. To avoid this, it is necessary to understand the physics behind crack growth and look for the true

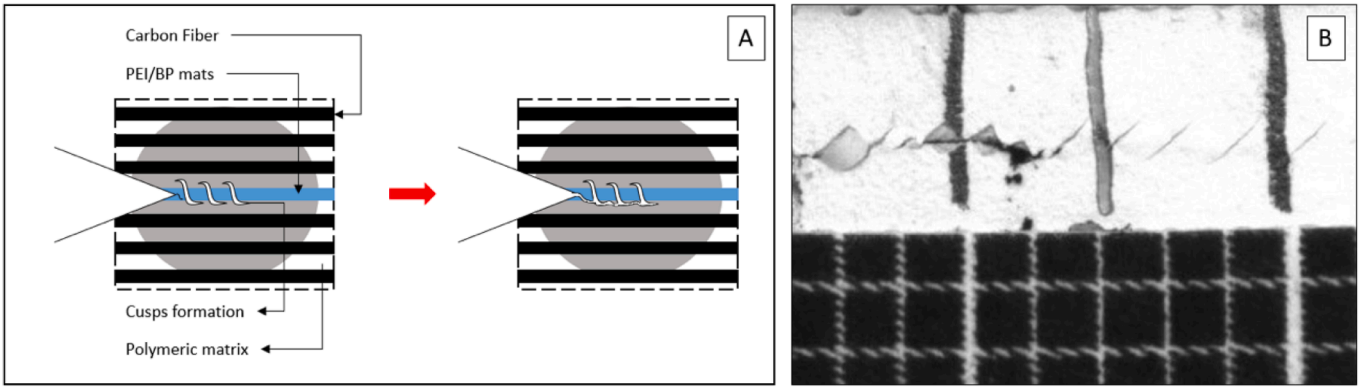

Fig. 16. (A) Cusps formation and their coalescence during the ENF test, and (B) cusps aspects observed at the side of the specimen during the ENF tests.

growth or the crack, to allow correlating micro and macroscopic delamination growth. In this work, the dissipation energy values (as from physics) for mode I and mode II are different according to the dU/increment vs da/increment curve observed for each test. The phenomenon of crack link-up in mode II is characterized by a lower energy cost, whereas the buckypaper exhibits an increase in energy consumption. Moreover, beyond the threshold energy, it is expected that mode II is inferior to mode I, as crack propagation requires a higher energy input for successful link-up. However, the bridging effect of buckypapers in mode II changes and shifts the curve to higher values. The confinement of the process zone in mode-I remains within BP, which is observed in the microscopies presented in Fig. 8. Hence, on both surfaces there are fracture mechanisms related to buckypaper failure and for high magnification carbon nanotubes are clearly seen. While, in mode II the shear cracks (cusps formation) are bridged by buckypaper shifting the energy to high values, and plastic deformation caused by this bridging effect is observed in Fig. 14.

According to the collected results, buckypaper mats improved the interlaminar toughness under the mode-II test. In this case, the crack propagated following shear forces ahead of the crack tip [7]. Thus, the crack propagates because of micro-cracks, striations, and cusps (visually observed) and their coalescence, as schematically presented in Fig. 16A. Also, the cusps formation was observed during the experimental test on the observed surface, as observed in Fig. 16B. The way the crack develops in mode-II, is in accordance with Amaral et al [40]. Also, they observed an angle of approximately −80° in the initial crack. The BP mats acted as a bridge connection in this case, which hindered and modified how the cracks propagated. Hence, more energy was required to break bonds to overcome the interfacial change in crack direction from the BP mats region to the thermoplastic matrix. Consequently, the nanofiller strengthened the interlaminar toughness of the composites [15].

4. Conclusions

This work evaluates the carbon nanotube buckypaper effect on the interlaminar toughness of PEI and PAEK composites under opening and shear quasi-static delamination loading. Based on the results, the incorporation of buckypaper promoted an enhancement of mode-II once the BP created an easy pathway for crack propagation for mode-I tests. This behavior can be attributed to how the crack grows in the composite. In mode-I, the crack tends to propagate straight, growing inside the buckypaper, which creates an easy pathway to growth and reduces the interlaminar toughness. This behavior was physically explained by the smoother fractured surface on BP mats, resulting in lower damage features and lower interfacial resistance. Inside the buckypaper, carbon nanotubes bonded by van der Waals forces remained weaker than the strong covalent bonds at the interface region. For mode-II, the matrix squeeze inside the buckypaper did not negatively affect the crack propagation, because the crack tends to grow by the coalescence of cusps where the initial crack angle creates a rougher fracture surface, requiring more energy to modify the cohesive fracture between buckypapers/mats and matrix. Therefore, carbon nanotubes acted as a bridge, and the buckypaper was dragged, consuming more energy and shifting the interlaminar toughness to high values on shear mode. Considering the difference between mode-I and mode-II results, the crack propagation behavior using BP mats is dependent on the loading mode applied. The loading mode affects the process zone ahead of the crack tip with distinctively different behavior beyond ‘onset’ (growth versus link-up), which defines the physical behavior of crack growth. Therefore, for laminated composites reinforced with nano reinforcements (buckypapers in this case), it is extremely important to perform both tests (mode-I and mode-II) together to properly understand the interlaminar toughness and better define its final application.

CRediT authorship contribution statement

Luis Felipe de Paula Santos: Conceptualization, Methodology, Validation, Investigation, Writing – original draft. **Francisco Maciel Monticeli:** Conceptualization, Methodology, Validation, Writing – original draft. **Bruno Ribeiro:** Conceptualization, Methodology, Writing – review & editing, Supervision. **Michelle Leali Costa:** Conceptualization, Validation, Writing – review & editing, Supervision. **René Alderliesten:** Validation, Writing – review & editing, Supervision. **Edson Cocchieri Botelho:** Conceptualization, Validation, Writing – review & editing, Supervision.

Declaration of Competing Interest

The authors declare that they have no known competing financial interests or personal relationships that could have appeared to influence the work reported in this paper.

Data availability

The authors do not have permission to share data.

Acknowledgments

The authors are grateful for the financial support given by the Brazilian Funding Institutions: São Paulo Foundation Research (FAPESP) (2018/07867-3, 2019/18691-6, and 2021/05706-5), National Council for Scientific and Technological Development (CNPq) (140852/2018-2, 306576/2020-1 and 304876/2020-8) and this study was financed in part by the Coordenação de Aperfeiçoamento de Pessoal de Nível Superior – Brasil (CAPES) – Finance Code 001.

References

[1] Pini T, Caimmi F, Briatico-Vangosa F, Frassine R, Rink M. Fracture initiation and propagation in unidirectional CF composites based on thermoplastic acrylic resins. Eng Fract Mech 2017;184:51–8. https://doi.org/10.1016/j.engfracmech.2017.08.023.

[2] Sauer M, Kühnel M, Elmar W. Report - Composites Market Report 2018 - Market developments, trends, outlook and challenges. Carbon Composites 2018;1–44.

[3] Stewart R. Thermoplastic composites - Recyclable and fast to process. Reinf Plast 2011;55:22–8. https://doi.org/10.1016/S0034-3617(11)70073-X.

[4] Wang S, Downes R, Young C, Haldane D, Hao A, Liang R, et al. Carbon Fiber/Carbon Nanotube Buckypaper Interply Hybrid Composites: Manufacturing Process and Tensile Properties. Adv Eng Mater 2015;17:1442–53. https://doi.org/10.1002/adem.201500034.

[5] Eskizeybek V, Yar A, Avcı A. CNT-PAN hybrid nanofibrous mat interleaved carbon/epoxy laminates with improved Mode I interlaminar fracture toughness. Compos Sci Technol 2018;157:30–9. https://doi.org/10.1016/j.compscitech.2018.01.021.

[6] Amaral L, Yao L, Alderliesten R, Benedictus R. The relation between the strain energy release in fatigue and quasi-static crack growth. Eng Fract Mech 2015;145:86–97. https://doi.org/10.1016/j.engfracmech.2015.07.018.

[7] Srivastava VK, Gries T, Veit D, Quadflieg T, Mohr B, Kolloch M. Effect of nanomaterial on mode I and mode II interlaminar fracture toughness of woven carbon fabric reinforced polymer composites. Eng Fract Mech 2017;180:73–86. https://doi.org/10.1016/j.engfracmech.2017.05.030.

[8] Kumar M, Bhowmik S, Balachandran M, Abraham M. Composites : Part A Effect of surface functionalization on mechanical properties and decomposition kinetics of high performance polyetherimide / MWCNT nano composites. Compos A 2016;90:147–60. https://doi.org/10.1016/j.compositesa.2016.06.025.

[9] Chetehouna K, Hamamda S, Gascoin N, Revo S. : Preparation and characterization of polytetra fl uoroethylene (PTFE)/ Thermally Expanded Graphite (TEG) nanocomposites 2017;124:175–81.

[10] Ashuri M, He Q, Liu Y, Emani S, Shaw LL. Synthesis and performance of nanostructured silicon/graphite composites with a thin carbon shell and engineered voids. Electrochim Acta 2017;258:274–83. https://doi.org/10.1016/j.electacta.2017.10.198.

[11] Zabihi O, Ahmadi M, Nikafshar S, Chandrakumar Preyeswary K, Naebe M. A technical review on epoxy-clay nanocomposites: Structure, properties, and their applications in fiber reinforced composites. Compos B Eng 2018;135:1–24. https://doi.org/10.1016/j.compositesb.2017.09.066.

[12] Vorobei AM, Pokrovskiy OI, Ustinovich KB, Parenago OO, Savilov SV, Lunin VV, et al. Preparation of polymer e multi-walled carbon nanotube composites with enhanced mechanical properties using supercritical antisolvent precipitation 2016;95:77–81.

[13] Dalcanale F, Grossenbacher J, Blugan G, Gullo MR, Brugger J, Tevaearai H, et al. Rapid carbon nanotubes suspension in organic solvents using organosilicon polymers. J Colloid Interface Sci 2016;470:123–31. https://doi.org/10.1016/j.jcis.2016.02.050.
[14] Dydek K, Latko-Duralek P, Boczkowska A, Sałaciński M, Kozera R. Carbon Fiber Reinforced Polymers modified with thermoplastic nonwovens containing multi-walled carbon nanotubes. Compos Sci Technol 2019;173:110–7. https://doi.org/10.1016/j.compscitech.2019.02.007.
[15] Melly SK, Peng T, Di Zhao Q, de Ji S, Li YC, Wang G, et al. Interlaminar properties of GFRP laminates toughened by CNTs buckypaper interlayer. Compos Struct 2018;208:13–22. https://doi.org/10.1016/j.compstruct.2018.10.002.
[16] Han J, Zhang H, Chen M, Wang D, Liu Q. The combination of carbon nanotube buckypaper and insulating adhesive for lightning strike protection of the carbon fiber / epoxy laminates. **4** (2015).
[17] Pons F, Cinquin J. Enhancement of electrical conductivity of composite structures by integration of carbon nanotubes via bulk resin and / or buckypaper fi lms. **122**, 31–40 (2017).
[18] Liu L, Shen L, Zhou Y. Improving the interlaminar fracture toughness of carbon/epoxy laminates by directly incorporating with porous carbon nanotube buckypaper. J Reinf Plast Compos 2016;35:165–76. https://doi.org/10.1177/0731684415610919.
[19] Chen C, Li Y, Yu T. Interlaminar toughening in flax fiber-reinforced composites interleaved with carbon nanotube buckypaper. J Reinf Plast Compos 2014;33:1859–68. https://doi.org/10.1177/0731684414548084.
[20] Shin YC, Kim SM. Enhancement of the interlaminar fracture toughness of a Carbon-Fiber-Reinforced polymer using interleaved carbon nanotube Buckypaper. Applied Sciences (Switzerland) 2021;11. https://doi.org/10.3390/app11156821.
[21] Yazdanparast R, Rafiee R. Investigating the influence of pull-out speed on the interfacial properties and the pull-out behavior of CNT/polymer nanocomposites. Compos Struct 2023;316:117049. https://doi.org/10.1016/j.compstruct.2023.117049.
[22] Rafiee R, Sahraei M. Characterizing delamination toughness of laminated composites containing carbon nanotubes: Experimental study and stochastic multi-scale modeling. Compos Sci Technol 2021;201:108487. https://doi.org/10.1016/j.compscitech.2020.108487.
[23] Santos LF de P, Alderliesen R, Kok W, Ribeiro B, Bovi J de O, et al. The influence of carbon nanotube buckypaper / poly (ether imide) mats on the thermal properties of poly (ether imide) and poly (aryl ether ketone)/ carbon fiber laminates. **116** (2021). http://doi:10.1016/j.diamond.2021.108421.
[24] ASTM D5528-01: Standard test method for mode I interlaminar fracture toughness of unidirectional fiber-reinforced polymer matrix composites. American Standard of Testing Methods, **03**, 1–12 (2014). http://doi:10.1520/D5528-13.2.
[25] ASTM D7905: Standard test method for determination of the mode II interlaminar fracture toughness of unidirectional fiber-reinforced polymer matrix composites. Astm, , 1–18 (2014). http://doi:10.1520/D7905.
[26] Lee SH, Kim H, Hang S, Cheong SK. Interlaminar fracture toughness of composite laminates with CNT-enhanced nonwoven carbon tissue interleave. Compos Sci Technol 2012;73:1–8. https://doi.org/10.1016/j.compscitech.2012.09.011.
[27] Griffith AA. VI. The phenomena of rupture and flow in solids. Philosophical Transactions of the Royal Society of London. Series A, Containing Papers of a Mathematical or Physical Character, **221**, 163–198 (1921). http://doi:10.1098/rsta.1921.0006.
[28] Amaral L, Zarouchas D, Alderliesten R, Benedictus R. Energy dissipation in mode II fatigue crack growth. Eng Fract Mech 2017;173:41–54. https://doi.org/10.1016/j.engfracmech.2017.01.020.
[29] Alderliesten RC. How proper similitude can improve our understanding of crack closure and plasticity in fatigue. Int J Fatigue 2016;82:263–73. https://doi.org/10.1016/j.ijfatigue.2015.04.011.
[30] Stemp WJ, Macdonald DA, Gleason MA. Testing imaging confocal microscopy, laser scanning confocal microscopy, and focus variation microscopy for microscale measurement of edge cross-sections and calculation of edge curvature on stone tools: Preliminary results. J Archaeol Sci Rep 2019;24:513–25. https://doi.org/10.1016/j.jasrep.2019.02.010.
[31] Amaral L, Alderliesten R, Benedictus R. Towards a physics-based relationship for crack growth under different loading modes. Eng Fract Mech 2018;195:222–41. https://doi.org/10.1016/j.engfracmech.2018.04.017.
[32] Al-Khudairi O, Hadavinia H, Waggott A, Lewis E, Little C. Characterising mode I/mode II fatigue delamination growth in unidirectional fibre reinforced polymer laminates. Mater Des 2015;66:93–102. https://doi.org/10.1016/j.matdes.2014.10.038.
[33] Greenhalgh ES. Delamination-dominated failures in polymer composites. In *Failure Analysis and Fractography of Polymer Composites*; Elsevier, (2009); pp. 164–237.
[34] Li Z, Wang Y, Cao J, Meng X, Aamir RM, Lu W, et al. Effects of loading rates on mode I interlaminar fracture toughness of carbon/epoxy composite toughened by carbon nanotube films. Compos B Eng 2020;200:108270. https://doi.org/10.1016/j.compositesb.2020.108270.
[35] Monticeli FM, Odila Hilário Cioffi M, Jacobus Cornelis Voorwald H. Mode II delamination of carbon-glass fiber/epoxy hybrid composite under fatigue loading. Int J Fatigue, 2021;154:106574. http://doi:10.1016/j.ijfatigue.2021.106574.
[36] Chen J, Yan L, Song W, Xu D. Interfacial characteristics of carbon nanotube-polymer composites: A review. Compos A Appl Sci Manuf 2018;114:149–69. https://doi.org/10.1016/j.compositesa.2018.08.021.
[37] Khan SU, Kim J-K. Improved interlaminar shear properties of multiscale carbon fiber composites with bucky paper interleaves made from carbon nanofibers. Carbon 2012;50:5265–77. https://doi.org/10.1016/j.carbon.2012.07.011.
[38] Ayatollahi MR, Pavier MJ, Smith DJ. Determination of T -stress from finite element analysis for mode I and mixed mode I/II loading. Int J Fract 1998;91:283–98. https://doi.org/10.1023/A:1007581125618.
[39] Khan R, Alderliesten R, Badshah S, Khattak MAS, Khan M, Benedictus R. EXPERIMENTAL INVESTIGATION OF THE MICROSCOPIC DAMAGE DEVELOPMENT AT MODE I FATIGUE DELAMINATION TIPS IN CARBON/EPOXY LAMINATES. Jurnal Teknologi, **78** (2016). http://doi:10.11113/.v78.8072.
[40] Daneshjoo Z, Amaral L, Alderliesten RC, Shokrieh MM, Fakoor M. Development of a physics-based theory for mixed mode I/II delamination onset in orthotropic laminates. Theor Appl Fract Mech 2019;103:102303. https://doi.org/10.1016/j.tafmec.2019.102303.